A chemometric-assisted voltammetric analysis of free and Zn(II)-loaded metallothionein-3 states

PERIS-DÍAZ, M.D.; RICHTERA, L.; ZÍTKA, O.; KREŻEL, A.; ADAM, V

Bioelectrochemistry
2020, vol. 134, August 2020, pp. 1-8

ISSN: 1567-5394

DOI: https://doi.org/10.1016/j.bioelechem.2020.107501

Accepted manuscript

A chemometric-assisted voltammetric analysis of free and Zn(II)-loaded metallothionein-3 states

Manuel David Peris-Díaz,[a] Lukas Richtera,[b,c] Ondrej Zitka,[b,c] Artur Krężel,[a] and Vojtech Adam[b,c]*

[a] *Department of Chemical Biology, Faculty of Biotechnology, University of Wrocław, F. Joliot-Curie 14a, 50-383 Wrocław, Poland*

[b] *Department of Chemistry and Biochemistry, Mendel University in Brno, Zemedelska 1, 613 00 Brno, Czech Republic*

[c] *Central European Institute of Technology, Brno University of Technology, Purkynova 123, 612 00 Brno, Czech Republic*

***Corresponding author**

Vojtech Adam, Department of Chemistry and Biochemistry, Mendel University in Brno, Zemedelska 1, CZ-613 00 Brno, Czech Republic; E-mail: vojtech.adam@mendelu.cz; phone: +420-5-4513-3350; fax: +420-5-4521-2044

Abstract

We focused on the application of mass spectrometry and electrochemical methods combined with a chemometric analysis for the characterization of partially loaded Zn(II) MT3 species. The results showed decreased Cat1 and Cat2 signals for the Zn(II)-loaded MT3 species with respect to the metal-free protein, which might be explained by the arrangement of tetrahedral metal-thiolate coordination environments and the formation of metal clusters. Moreover, there was a decrease in the Cat1 and Cat2 signals, and a plateau was reached with 4-5 Zn(II) ions that corresponded to the formation of the C-terminal α-domain. Regarding the Zn_{7-x}MT3 complexes, we observed three different electrochemical behaviours for the $Zn_{1–2}$MT3, $Zn_{3–6}$MT3 and Zn_7MT3 species. The difference for $Zn_{1–2}$MT3 might be explained by the formation of independent ZnS_4 cores in this stage that differ with respect to the formation of Zn_xCys_y clusters with an increased Zn(II) loading. The binding of the third Zn(II) ion to MT3 resulted in high sample heterogeneity due the co-existence of $Zn_{3–6}$MT3. Finally, the Zn_7MT3 protein showed a third type of behaviour. The fact that there were no free Cys residues might explain this phenomenon. Thus, this research identifies the major proteins responsible for zinc buffering in the cell.

Keywords: Metallomics; voltammetry; metal ions; chemometrics

Highlights

- Study of Zn(II)-loaded metallothionein-3 by voltammetric and chemometric analyses.
- Electrochemical signals differed between the metal-free and metal-loaded MT3 species.
- Zn–S networks were arranged differently for variously loaded $Zn_{1–7}$MT3 species.
- $Zn_{1–2}$MT3, $Zn_{3–6}$MT3 and Zn_{7}MT3 were differentiated by PCA and PLS analyses.
- Novel electrochemical signals were found to differentiate the protein species.

1. Introduction

Metallothioneins (MTs) are a heterogeneous superfamily of ubiquitous cysteine-rich and low-molecular-weight proteins dispersed among all major kingdoms. Four isoforms (MT1-4) with multiple subisoforms are characteristic of mammalian MTs (mMTs) [1-3]. Their high cysteine content, which is ~ 30% of all the amino acid residues in the protein sequence, provides the capability for binding various metal ions (physiological and toxic) and for the formation of metal-thiolate clusters [1, 4]. However, it has been recognized that mMTs are involved in zinc and copper metabolism under normal conditions. Commonly, mMTs when bound to divalent metal ions (M) exhibit two separate domains, the N-terminal (β) with M_3Cys_9 and the C-terminal (α) with M_4Cys_{11} clusters. Interestingly, in other MT families, the number of domains or metal ions at each cluster differs [4, 5]. Metal-binding preferences vary between the mMT isoforms with regard to Cu(I) and Zn(II) ions. For instance, MT1 and MT2 isoforms are ubiquitously expressed and perform multiple physiological functions, including maintaining zinc homeostasis with varying metal binding abilities [6]. On the other hand, MT3 is mainly localized in the central nervous system, modulating neuronal zinc and copper metabolism [2, 7]. Because of its cellular function, it is naturally isolated as a mixture of Cu(I)/Zn(II) complexes [2, 7, 8]. A study of the structure-to-function relationship is of vital importance to understand the existence of a high number of isoforms and subisoforms and their physiological and pathological importance [9]. In addition, the metal saturation degree regulates and buffers the free metal concentration of the cell [10, 11]. Previous spectroscopic and isothermal titration calorimetry (ITC) methods have determined the Zn(II) binding affinities for MT2 and MT3, and they revealed nano- and pico-molar affinities [12, 13]. These findings implicate that partially unsaturated Zn_{4-6}MT species are important for the processes of zinc buffering and muffling in the cell [14-16]. The isolation and study of particular metal-depleted Zn_{7-x}MT species is hampered by common biophysical methods due to the lack of secondary structures

and aromatic amino acids. In addition to the highly disordered and dynamic protein behaviour, the silent spectroscopic character of Zn(II) and Cu(I) exacerbates the issue [4, 7, 17]. Currently, the use of native mass spectrometry (native MS) to preserve the non-covalent interactions of proteins from solution has become routine [18-21]. Thus, information about protein conformation and metal-ion coordination is easily obtained [22]. Several MS reports have indicated the co-existence of several partially loaded states of Zn(II)/Cu(I) or Zn(II)/Cd(II) in MTs [23-29]. Nonetheless, the MS signal does not always provide a direct quantification of the metal-to-protein concentration or stoichiometry [30]. Metal deposition or supermetallation are processes that might occur in ESI-MS under certain conditions, and consequently, special care must be taken when studying protein metalation states [31, 32]. Therefore, it is of great interest to develop complementary tools that may provide new insights. Electrochemical methods have been applied in metallothionein studies; however, an interpretation of the voltammograms is rather complicated [33-37]. To solve this, multivariate curve resolution (MCR)-assisted voltammetry provides a way to interpret them [34, 38]. One sensitive method that has been widely applied in the past to quantify MT levels and separate MT isoforms is the Brdicka reaction [39, 40]. This electrochemical method measures the catalytic signal of hydrogen evolution catalysed by a protein with free RSH groups in a Co(III) complex solution. The obtained voltammogram is characterized by three main peaks: RS_2Co (-1.25 V), Cat1 (-1.40 V) and Cat2 signals (-1.55 V) that correspond to the hydrogen evolution from the electrolyte catalysed by MT and to the two interactions of the MT-Brdicka electrolyte components, respectively [41]. For RSH quantification purposes, Cat2 demonstrated good analytical parameters. Different electrochemical behaviours were encountered for the MT subisoforms and isoforms and between the MT species [42-47]. Moreover, electrochemical changes of apo-MT2 and apo-MT3 after a full metal loading with 7 eq. of Cd(II) and Pb(II) have been reported [48].

To the best of our knowledge, the Brdicka reaction has not been applied to differentiate the Zn(II)-loading status of MTs, and only native MS has been used to investigate coexisting metal complex species. This research aimed to characterize and find differences in the electrochemical behaviour of free and partially Zn(II)-loaded MT3 species ($Zn_{0–7}MT3$). The approach presented in this article provides a complementary methodology for studying the binding of metal ions to disordered proteins.

2. Experimental

2.1 Materials

The following reagents were purchased from Sigma-Aldrich (Merck): $ZnSO_4 \cdot 7H_2O$, $(CdSO_4)_3 \cdot 8H_2O$, NH_4Cl, NH_3(aq), $[Co(NH_3)_6]Cl_6$, 4-(2-pyridylazo)resorcinol (PAR), $(NH_4)_2CO_3$, tris(hydroxymethyl)aminomethane (Tris base), 4-(2-hydroxyethyl)-1 piperazineethanesulfonic acid (HEPES), tris(2-carboxyethyl)phosphine hydrochloride (TCEP), ammonium acetate, 2,5-dihydroxybenzoic acid (DHB), ethylenediaminetetraacetic acid (EDTA), methanol (mass spectrometry grade), and acetonitrile (ACN, mass spectrometry grade). The metal-chelating resin Chelex 100 was acquired from Bio-Rad, and 98% hydrochloric acid (HCl) was purchased from VWR Chemicals. Tryptone, yeast extract, LB broth, agar, agarose, isopropyl-β-D-1-thiogalactopyranoside (IPTG), and SDS were obtained from Lab Empire; NaCl, NaOH, glycerol, $KH_2PO_4 \cdot H_2O$, and K_2HPO_4 were obtained from POCH (Gliwice Poland); pTYB21 vector and chitin resin were obtained from New England BioLabs; and 5,5'- dithiobis-(2-nitrobenzoic acid) (DTNB) was obtained from TCI Europe. Dithiothreitol (DTT) and trifluoroacetic acid (TFA) were purchased from Iris Biotech GmbH.

2.2 Expression, purification and reconstitution of metallothionein-3

The cDNAs encoding human MT3 were purchased from GenScript and cloned into the pTYB21 vector (New England Biolabs), which was deposited in the Addgene plasmid repository (https://www.addgene.org) as plasmid ID 105710 (MT3) [24]. Expression vectors were transformed into BL21(DE3)pLysS *E. coli* cells and cultured in a rich full culture medium (1.1% tryptone, 2.2% yeast extract, 0.45% glycerol, 1.3% K_2HPO_4, 0.38% KH_2PO_4, all *w*/*w*) at 37 °C until 0.5 OD_{600} [49]. Cells were induced with 0.1 mM IPTG and incubated overnight at 20 °C with vigorous shaking. Next, purification steps were conducted at 4 °C. Cells were collected by centrifugation (4,000 *g*, 10 min), resuspended in 50 ml of cold buffer A (20 mM HEPES, pH 8.0, 500 mM NaCl, 1 M EDTA, 1 mM TCEP) and sonicated for 30 min (1 min "on" and 1 min "off") followed by centrifugation (20,000 *g*, 15 min) [50]. The supernatant was incubated with 20 ml of chitin resin in buffer A and kept overnight with mild shaking. After the incubation, the resin was washed 4-5 times with 50 ml of buffer A, and cleavage was induced by the addition of 100 mM DTT and incubation for 48 h at room temperature on a rocking bed. The eluted solution was acidified to pH ~ 2.5 with 7% HCl (*v*/*v*) and concentrated using Amicon Ultra-4 Centrifugal Filter Units with a membrane cut-off of 3 kDa (Merck). Then, the solution was purified on a size exclusion chromatography SEC-70 gel filtration column (Bio-Rad) equilibrated with 10 mM HCl. The identity of apo-MT3 protein (thionein) was confirmed by ESI-MS (API 2000 instrument, Applied Biosystems). The concentration of thiols was determined spectrophotometrically using the DTNB assay [51]. The protein binding capacity was confirmed spectrophotometrically by Zn(II) and Cd(II) titrations [13]. Purified thionein was mixed with a 10 molar excess of $ZnSO_4$ under a nitrogen blanket, and the pH was adjusted to 8.6 with a 1 M solution of Tris base. The sample was concentrated with Amicon Ultra-4 Centrifugal Filter Units, containing a membrane cut-off of 3 kDa (Merck), and purified on an SEC-70 gel filtration column (Bio-Rad) equilibrated with 10 mM Tris-HCl buffer at pH 8.6. The concentrations of thiols and Zn(II) were determined spectrophotometrically using DTNB

and PAR assays, respectively [51, 52]. $Zn_{0–7}$MT3 samples were obtained by lowering to pH ~ 2.5 with 7% HCl (*v*/*v*) of Zn_7MT3 stock and separated on an SEC-70 gel filtration column (Bio-Rad) with 10 mM HCl. Different amounts of $ZnSO_4$ were added to apoMT3 and desalted using an Amicon Ultra-4 Centrifugal Filter (3K) to finally obtain the $Zn_{0–7}$MT3 samples.

2.3 Direct injection electrospray ionization-mass spectrometry (DI-ESI-MS)

A Bruker Maxis Impact (Bruker Daltonik GmbH, Bremen, Germany) instrument was used for the native ESI-MS analysis. Aliquots of $Zn_{0–7}$MT3 were diluted with 50 mM ammonium acetate and 10% methanol (*v*/*v*, pH 7.4) to a final concentration of 15 μM and then were injected directly by a syringe pump with a 2 μl/min flow rate. The following mass spectrometer parameters were used: end plate offset potential 500 V; capillary potential 4000 V; nebulizer gas (N_2) pressure 1.5 bar; drying gas (N_2) flow rate 4 l/min; drying temperature 180 °C. The mass range was set from 50 to 3000 m/z. Prior to analysis, the mass spectrometer was calibrated using a commercial ESI-TOF tuning mix (Merck).

2.4 MALDI-TOF analysis

The mass spectra were acquired with a MALDI-TOF/TOF MS Bruker UltrafleXtreme (Bruker Daltonik GmbH, Bremen, Germany) instrument. The instrument was controlled by flexControl v3.4 and flexAnalysis v3.4 software (Bruker Daltonik GmbH, Bremen, Germany). The DHB matrix was used as the MALDI-TOF matrix for protein analysis. The saturated matrix solution was prepared with 30% acetonitrile and 0.1% trifluoroacetic acid. The MALDI-MS analysis of proteins was performed in a linear positive mode with a 2–20 kDa range. The mass spectra were typically acquired by averaging 2,000 subspectra from a total of 2,000 laser shots per spot. The laser power was set to 5−10% above the threshold. The calibration was performed using a standard peptide and protein calibration mixture obtained from Bruker Daltonik GmbH.

2.5 Determination of metallothionein by the Brdicka solution

Electrochemical determination of metallothionein-3 was performed using an 884 Professional VA potentiostat/galvanostat (Metrohm AG, Herissau, Switzerland) connected to an 889 IC Sample Center autosampler (Metrohm AG, Herissau, Switzerland) controlled with Viva v2.0 and MagIC NET v3.1 software (Metrohm AG, Herissau, Switzerland). Viva v2.0 software was also used for raw data processing. An electrolyte stock solution and electrochemical cell were cooled to 4 °C using a Julabo F25 (JULABO GmbH, Seelbach, Germany) instrument during storage and measurements. Before dosing, samples were stored at 5 °C using the 889 IC Sample Center autosampler. Differential pulse voltammetry measurements were performed using a standard three-electrode system with a hanging mercury drop electrode as the working electrode (drop area of 0.4 mm^2), and Ag/AgCl/3 M KCl and a platinum electrode were used as the reference and auxiliary electrode, respectively. An electrolyte with a dosed sample (exchanged after each measurement) was deoxygenated prior to measurement by purging with 99.999% argon (Messer Technogas, Brno, Czech Republic) for 20 s. As a supporting electrolyte, the Brdicka solution (1 mM $[Co(NH_3)_6]Cl_3$ in 1 M ammonia buffer (NH_3(aq) + NH_4Cl, pH 9.6) was used. The parameters of the metallothionein determination were as follows: (i) a potentiostatic pre-treatment was carried out with a stirring time of 5 s, a stirring rate of 2,000 min^{-1}, a start potential of -0.70 V, and a wait time of 60 s, (ii) sweep with a start potential of -0.70 V, an end potential of -1.75 V, a potential step of 0.003 V, a potential step time of 0.45 s, a sweep rate of 0.007 V/s, a pulse amplitude of 0.025 V, a pulse time of 0.04 s, a measuring time of 0.02 s, and a sweep duration of 157.5 s. The lowest current measuring range was set to 2 μA, and the highest measuring range was 2 mA. The volume of the dosed electrolyte was 4.5 ml (a dosing rate of 4 ml/min), and the volume of the injected sample of diluted Zn_{0-7}MT3 was between 1.0–27 μl, with an increment of 3.0 μl for each of the following

set of measurements (30 µl of a Zn_{0-7}MT3 stock solution was diluted with 1470 µl of Milli-Q water prior to use for the electrochemical measurements). Each Zn_{0-7}MT3 concentration measurement was repeated six times.

2.6 Chemometrics analysis

Four pre-treatment combinations were performed thorough this work: i) scaling by mean centring combined with unit variance (auto-scaling) [53]; ii) multiple scatter correction (MSC) using a mean spectrum as a reference to correct the scatter was followed by auto-scaling [54]; iii) 1st derivative calculated by Savitzky-Golay filters [55] followed by auto-scaling and iv) 2nd derivative calculated by Savitzky-Golay filters followed by auto-scaling [56]. An exploratory analysis was carried out by a principal component analysis (PCA), while partial least squares (PLS) was used for building a classification model [57]. Although many PLS algorithms have been developed, there were three considered for this work, the original non-linear iterative partial least squares (NIPALS), kernel algorithms and a statistically inspired modification of the PLS algorithm SIMPLS [58]. In this work, we used the NIPALS algorithm to compute the PLS1 modelling [59]. Seven cross-validations were used to determine the optimum number of latent variables (LVs) using the Y explained variance (R^2) and the predictable Y ability (Q^2Y) [60]. An evaluation of their predictive performance and validation of the PLS models was achieved by several approaches. First, an evaluation by the cumulative Q^2Y metric evaluates the error between the predicted and theoretical response variable vector (y) value from the regression model and the cumulative R^2X that evaluates the goodness of fit. However, the use of the Q^2Y value as a diagnostic criterion is not recommended when the number of features highly exceeds the number of samples because it leads to overfitting problems [61]. To further validate the PLS model, permutation tests (n = 1,000) were performed by randomly permuting the response variable vector (y) and calculating the Q^2Y value [62]. Then, we can compare the

obtained permutated values with the original Q^2Y value and assess its significance. Using n = 1,000 for the permutation tests, we were able to assess whether the original model was significant at the 0.001 level (1/n). Variable importance in the projection (VIP) was employed as a variable selection method to elucidate those variables that boosted the accuracy for the developed PLS models [63]. A variable with a VIP score greater than one was considered relevant for the model. All analyses and plots were performed in R programming version 3.6.1 using the R packages "pls" and "ggplot2" [64, 65].

3. Results and Discussion

3.1 Electrochemical characterization of the apoform and partially Zn(II)-loaded MT3 species.

Previous research characterized metallothionein voltammograms according to three typical peaks: RS2Co peak (-1.25 V), Cat1 peak (-1.40 V) and Cat2 peak (-1.55 V) [48], which are shown in Fig. 1. Numerous previously published papers [39, 41, 42, 48, 66], demonstrated the usefulness of the Brdicka procedure for the detection and quantification of MT2 and MT3. One of the main aims of this study was to study the electrochemical behaviour of partially Zn(II)-loaded MT3 species ($Zn_{1–7}MT3$), which has been attributed to the role of homeostatic control of intracellular Zn(II) levels in the cell [13, 14]. The MALDI-MS analysis confirmed the purity of FPLC-purified apo-MT3 (Fig. S1A). Moreover, a set of aliquots with various Zn(II)-to-protein molar ratios were prepared. The metal-ion stoichiometry was assessed by native MS prior to electrochemical analysis (Fig. S1B).

As previously demonstrated, a decrease in the Cat2 peak height was observed with regard to the apo form and fully saturated Zn_7MT3 [48]. This decrease might be linked with the arrangement of the tetrahedral metal-thiolate coordination environments and the formation of metal clusters [67, 68]. Moreover, the voltammograms showed how the RS2Co peak and Cat1

peak shifted for the $Zn_{1–7}$MT3 proteins (Fig. 1A). We observed a continuous decrease in the peak heights (Cat1 and Cat2) until they reached a plateau with 5 Zn(II) ions; the above observation corresponded to the formation and saturation of the C-terminal α-domain with the Zn_4Cys_{11} cluster (Fig. 1B, Fig. S2). However, the use of peak heights (Cat1 or Cat2) did not reveal major differences between the metal-depleted species $Zn_{5–7}$MT3, which are considered responsible for cellular zinc buffering (Fig. 1B, inset, Fig. S2).

3.2 Integration of electrochemical studies with chemometrics.

The electrochemical behaviour between partially Zn(II)-loaded MT3 species seemed similar when visually inspected and analysed for the Cat1/Cat2 peak heights. Thus, we decided to employ a chemometric approach to overtake the limitations that might come from a manual data analysis. In the first step, voltammograms were divided into four intervals with regard to potential values, although the full voltammogram ranging from -0.8 to -1.7 V was also considered for modelling. Spectral data are usually correlated; thus, the use of potential windows instead of full spectra may reduce false positives and achieve better predictions [69]. Next, the reduced intervals and full spectrum were subjected to several pre-processing methods to improve the subsequent modelling. Signal processing has been demonstrated to be useful before statistical analysis because it improves the extraction of relevant features to feed into statistical models [70]. Once the data were pre-processed, an exploratory analysis using PCA was carried out. In fact, PCA-score plots are of very useful for an exploratory analysis to find patterns where the number of variables highly exceeds the number of samples in the study [57]. Once the exploratory analysis was performed, combinations of interval range spectra and pre-processing methods that led to maximum differences in the PCA-score plot were considered for further analysis by PLS. The constructed PLS models were validated by seven internal cross-validation tests and compared in terms of their predictive ability (Q^2Y), goodness of fit (R^2X)

and permutation tests. These metrics determined which interval of the spectrum and the pre-processing method led to better predictions. Finally, we extracted the discriminant features or potential values for the PLS model that achieved the best predictive performance. This variable selection was carried out through a VIP analysis of the PLS models, which allowed us to elucidate the potential values that promoted differences for the apo form and partially metal-loaded complexes.

3.3 Modelling Zn(II) metallothionein-3 complexes by a chemometric analysis

Initially, we considered modelling the electrochemical curves obtained by a simple criterion: the apo form *versus* Zn(II)-metallothionein complexes. The combination of pre-processing methods and voltammogram intervals was first examined by PCA analysis. The use of PCA-score plots may reveal natural data aggravation, and it is especially useful when the number of variables highly exceeds the number of samples [57]. In all cases, there were two clearly separated clusters that corresponded to the apo-MT3 and $Zn_{1–7}$MT3 protein species, as shown for auto-scaled data in Fig. 2A. The natural aggravation of the data was further assessed by PLS modelling, which showed a high performance for the assayed figures of merit and was independent of the pre-processing method applied and the voltammogram interval chosen (Tables S1-S4). However, when the data were scaled by mean centring combined with unit variance, the complex models requiring a low number of latent variables (LVs) were simplified. In all the constructed PLS models, high Q^2Y and R^2X values were obtained (Table 1). The PLS-score plot for the first and second LV for the full voltammogram clearly showed two separated groups that corresponded to the apo form and Zn_{7-1}MT3 complexes (Fig. 2B). Moreover, the permutation test (pQ^2Y) proved that the predictive ability was not randomly obtained and validated the performance achieved for all models [62], as shown in Fig. 2C. All four assayed intervals showed lower pQ^2Y values than their counterpart Q^2Y (Table 1). Interestingly, the

PLS models that comprised Cat1 (-1.2/-1.4 V) and Cat2 (-1.5/-1.7 V) peaks required only 1 LV in comparison to the three used by the full voltammogram; furthermore, all of them provided lower maximum values for pQ^2Y values. To elucidate the potential values that promoted differences for the apo form and metal-MT3 complexes, a variable selection was performed through a VIP analysis over the PLS models [63]. The potential values that achieved VIP values higher than 1.0 were extracted and analysed. As expected, the Cat2 peak (−1.57 V) provided the highest VIP value, indicating that this feature contributed the most to describing the PLS model (Fig. 3A). There was a decrease in the intensity of the Cat1 and Cat2 peaks for the MT3 Zn(II)-loaded complexes ($p < 0.0001$) (Fig. 3B-C). In addition, we identified a potential value (−0.8 V) that was not previously assigned but showed differences between the MT3 apo form and Zn(II)-loaded states ($p < 0.0001$) (Fig. 3D).

Considering such promising results, we further examined the possibility of building an effective classification model for the Zn(II) content in MT3 following a previous chemometric workflow. First, an unsupervised PCA was performed over full voltammograms of the Zn_1MT3 to Zn_7MT3 protein species, thus leading to a three-component model that explained 92% of the data variation. The PCA-score plot revealed the natural grouping structure of the data with three main clusters (Fig. 4A). One cluster was formed by Zn_7MT3, another cluster was formed by $Zn_{1–2}$MT3, and the last cluster was formed by a mixture of the $Zn_{3–6}$MT3 species. In a previous study, it was demonstrated how the binding of the third Zn(II) equivalent to MT2 resulted in high sample heterogeneity with the co-existence of species with various metal ions bound, more specifically the formation of the $Zn_{3–7}$MT2 species [24]. This agreed with our results for MT3, which showed the co-existence of the $Zn_{3–6}$MT3 species. Subsequently, a PLS analysis was conducted on the full and reduced interval voltammograms with a set of pre-processing methods. In this approach, the performance obtained for the PLS models highly varied according to the voltammogram interval and how it was processed (Table S5-S8). Overall, auto-

scaling and the 2nd derivative followed by auto-scaling gave the best results, although the 1st derivative provided the highest figures of merit (Table 2). Interestingly, the interval that isolated the Cat2 peak (-1.5/-1.7 V) yielded a poor predictive capability in this case, suggesting that Cat2 had no ability to discriminate between the group of constructed metal complexes. In contrast, the full or interval voltammograms that considered the Cat1 peak (-1.2/-1.4 V) achieved highly similar metrics. We observed that the PCA-score plot obtained with respect to the Cat1 peak interval led to intuitively clustered data with the proposed metal complexes (Fig. 4A-B, S3A-B). The PLS-score pots for both models showed distinguished clusters, with more pronounced clusters when using the full voltammogram interval (Fig. 4C-D, S3C-D). The predictive ability of both PLS models was validated by permutation tests that evidenced lower Q^2Y values for the permutated models in comparison to the Q^2Y values obtained for the original models (Fig. 4E-F, S3E-F). Moreover, we inspected the potential values where major differences relied on the classification of metal complexes by the VIP analysis over the PLS models. The extracted potential values with VIP $\geq$ 1 showed three main regions that are attributed to the Cat2, Cat1 and P peak regions from the voltammogram, although the highest VIP value was provided by the Cat1 peak region (-1.2/-1.4 V) (Fig. 5A). The distribution of the autoscaled intensity data for these peaks was shown by box plots (Fig. 5B-D). One-way analysis of variance (ANOVA) and pairwise comparisons by Tukey's HSD were performed to determine whether differences existed between the mean values of the groups in each peak region. For the Cat2 peak, there were differences ($p < 0.001$) between $Zn_{1-2}MT3$ and $Zn_{3-6}MT3$ and between $Zn_{3-6}MT3$ and Zn_7MT3; however, no significant differences were found between the mean values of the $Zn_{1-2}MT3$ and Zn_7MT3 groups (Fig. 5B). In the case of the Cat1 peak, all the groups exhibited differences ($p < 0.001$) between them (Fig. 5C). The last peak region, P, showed mean value differences ($p < 0.001$) between $Zn_{1-2}MT3$ and Zn_7MT3 and between $Zn_{3-6}MT3$ and Zn_7MT3. However, in this case, the differences were not significant among Zn_{1-}

$_2$MT3 and Zn$_{3–6}$MT3 (Fig. 5D). In fact, it was not surprising why the isolated interval -1.2/-1.4 V that corresponded to the Cat1 peak region yielded high PLS metrics (Table 2). In conclusion, the Cat1 peak region was able to distinguish between all three groups of proteins, whereas the other two peak regions that contributed to the PLS models showed incomplete mean differences for the groups. The strategy implemented herein demonstrated the usefulness of specific intervals from the voltammograms, which relied on differences between the most important metal-MT3 complexes. Thus, those indicators might be employed later to characterize the Zn(II) content in metallothionein proteins.

Conclusions

In this research, we studied the electrochemical behaviour of partially loaded Zn(II) metallothionein-3 species through the use of the Brdicka reaction coupled with a chemometric analysis. The importance of partially Zn(II)-saturated MT species has been previously highlighted because of their zinc buffering role in the cell. The methodology proposed herein allowed us to differentiate between metal-free and metal-loaded MT3 proteins. Electrochemical signals were attributed to the arrangement of tetrahedral ZnCys$_4$ coordination environments and the formation of Zn$_x$Cys$_y$ clusters. Moreover, using the methodology implemented, we modelled three types of electrochemical nature corresponding to partially saturated Zn$_{1–2}$MT3, Zn$_{3–6}$MT3 and Zn$_7$MT3 species. Their electrochemical differences might be explained by several phenomena: i) the formation of independent ZnCys$_4$ sites in the Zn$_{1–2}$MT3 species with respect to the formation of Zn$_x$Cys$_y$ clusters in the other species; ii) when considering high Zn(II)-loading states, the formation of Zn$_x$S$_y$ and the co-existence of multiple metal-saturated species led to the Zn$_{3–6}$MT3 species grouping together; and iii) fully loaded Zn$_7$MT3 does not contain a free Cys residue in comparison with Zn$_{3–6}$MT3, and thus, their electrochemical features differ. Previous research solved the Zn(II) binding mechanism and the molecular

events associated with the MT2 isoform through a combination of mass spectrometry and molecular dynamics simulations. The present research pointed out similar molecular events for the differentiation of the Zn_{7-x}MT3 complexes and concluded that MT2 and MT3 share a common Zn(II)-binding mechanism and speciation. The workflow employed here demonstrated an alternative and complementary approach to other structural and thermodynamics studies that are used for studying metal binding proteins.

Acknowledgements

This research has been financially supported by the European Research Council (ERC), under the European Union's Horizon 2020 research and innovation programme (grant agreement no. 759585); by the Ministry of Education, Youth and Sports of the Czech Republic, under the CEITEC 2020 project (LQ1601) and the National Sustainability Programme (project no. LO1609); and by the Polish National Science Centre (NCN) under Opus grant no. 2018/31/B/NZ1/00567.

Appendix A. Supplementary data

Supplementary data to this article can be found online at XXX

Table 1. Predictive performance of PLS-DA models for modelling the autoscaled voltammograms for the apo-MT3 and metallothionein-3 Zn(II)-loaded states.

Interval (V)	Pre-processing	R^2X	Q^2Y	pQ^2Y^a (mean/max)	LVs
-0.8/-1.7	Auto-scaling	0.94	0.85	-0.82/0.25	4
-0.8/-1.7	2nd derivative + auto-scaling	0.70	0.60	-0.41/0.38	2
-1.2/-1.4	Auto-scaling	0.99	0.88	-0.70/0.38	6
-1.2/-1.4	2nd der. + auto-scaling	0.94	0.75	-0.82/0.34	5

[a]Mean and maximum of 1000 Q^2Y values of the permutated PLS models.

Table 2. Predictive performance of the PLS-DA models for modelling the voltammograms for the Zn(II) metallothionein-3 complexes.

Interval (V)	R^2X	Q^2Y	pQ^2Y^a (mean/max)	LVs
-0.8/-1.7	0.97	0.98	-0.54/0.42	3
-1.5/-1.7	0.97	0.97	-0.05/0.397	1
-1.3/-1.5	0.99	0.98	-0.19/0.45	2
-1.2/-1.4	0.89	0.97	-0.08/0.39	1

[a]Mean and maximum of 1000 Q^2Y values of the permutated PLS models.

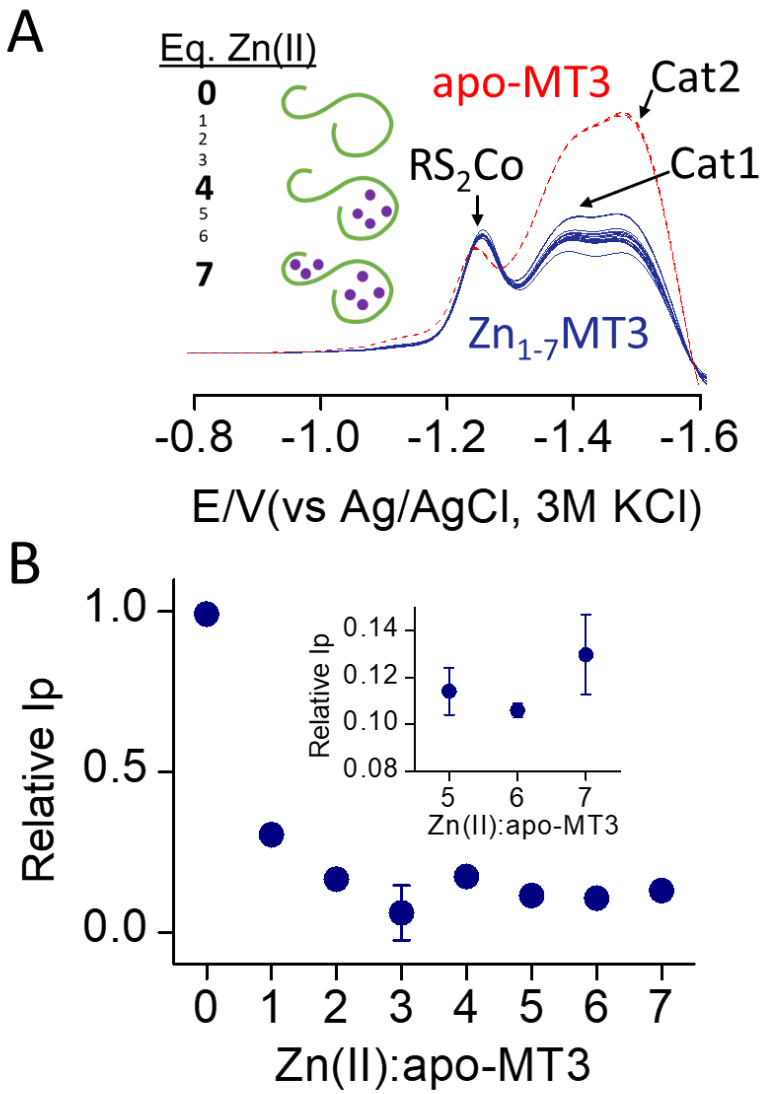

Figure 1. Protein preparation and electrochemical characterization. A) Inset: Schematic workflow for the preparation of the $Zn_{7-x}MT3$ protein complexes. Different molar equivalents of Zn(II) were added to the FPLC-purified apo-MT3 protein. Voltammogram obtained by differential pulse voltammetry in the Brdicka electrolyte for the apo-MT3 and $Zn_{1-7}MT3$ species. The typical characteristic peaks in the voltammogram (RS2Co, Cat1 and Cat2) are indicated. B) Relative peak height for Cat1 as a function of the number of Zn(II) ions.

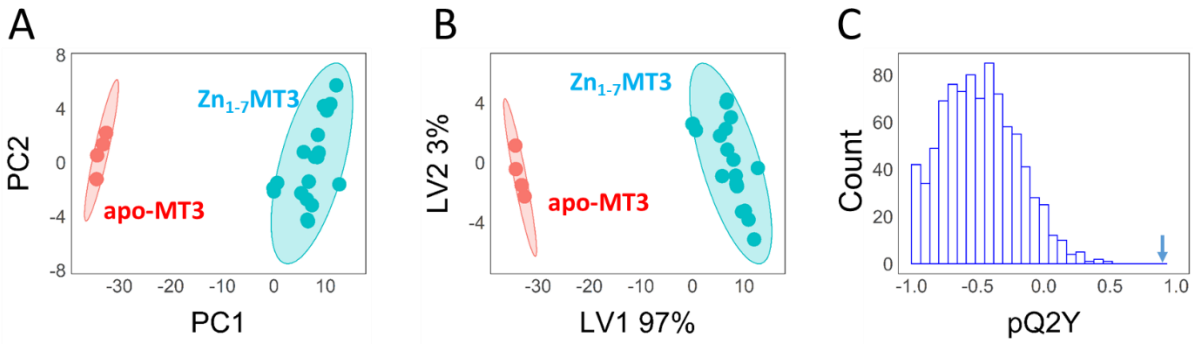

Figure 2. Chemometric analysis of the autoscaled voltammograms from the apo-MT3 vs $Zn_{1–7}$MT3 protein species. A) PCA-score plot obtained for the first and second principal components for the apo-MT3 and $Zn_{1–7}$MT3 complexes; B) PLS score plot from the PLS model considering the full voltammograms; C) density plot of the 1000 permutated Q^2Y values obtained for the PLS model built from considering the full voltammograms (-0.8 to -1.7 V). The arrow indicates the Q^2Y obtained for the model.

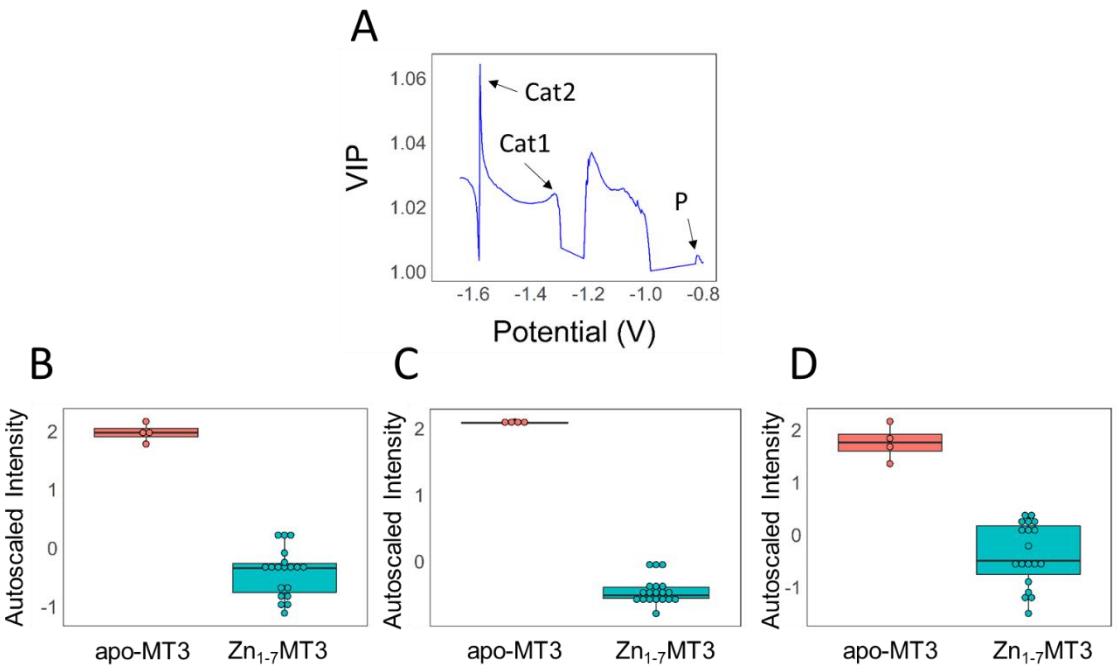

Figure 3. Variable importance projection (VIP) analysis of the PLS model considering full voltammograms of the apo- and metal-MT3 proteins. A) VIP values obtained for the voltammogram. The Cat1, Cat2 and P peaks are labelled; B) Box-plot of the Cat2 peak; C) Box-plot of the Cat1 peak; D) Box-plot of the P peak. The *y*-axis in the box plots refers to the autoscaled intensity.

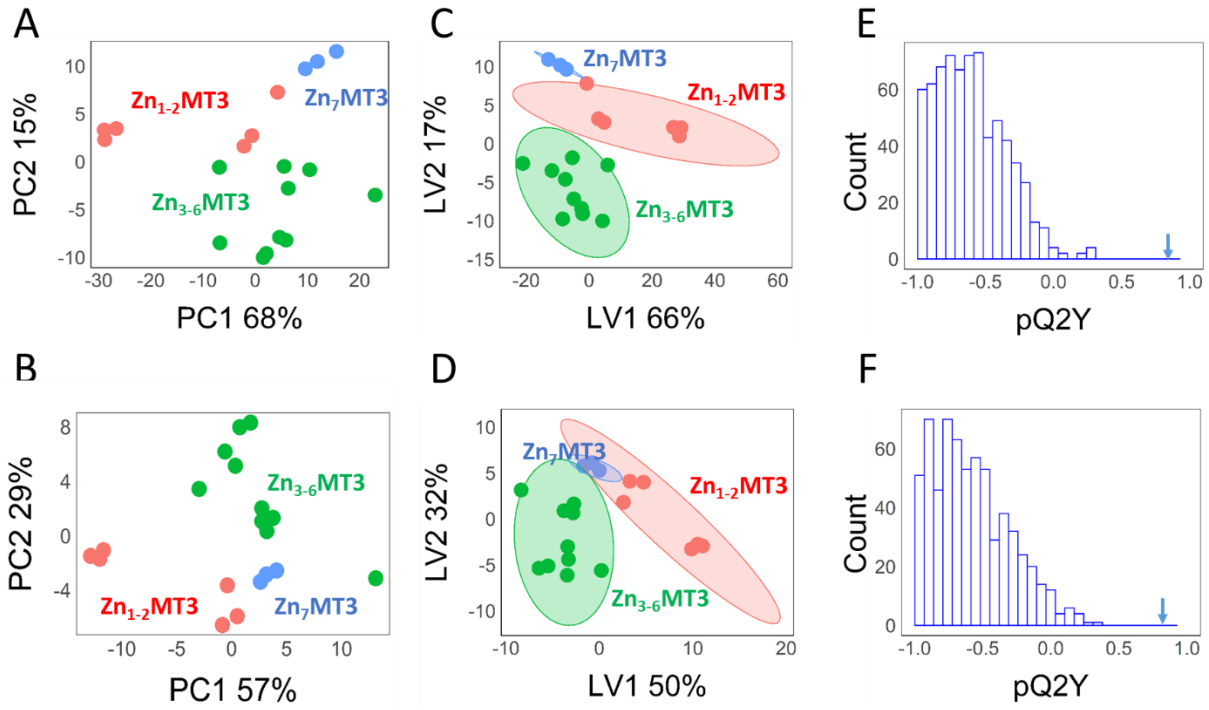

Figure 4. Chemometric analysis of the autoscaled voltammograms from the $Zn_{1–7}MT3$ complexes. A) PCA-score plot obtained for the first and second principal components in the full voltammogram; B) PCA-score plot obtained for the first and second principal components in the interval -1.2/-1.4 V; C) PLS- score plot from the PLS model considering the full voltammogram; D) PLS- score plot from the PLS model considering the interval -1.2/-1.4 V; E) Density plot of the 1,000 permutated-Q^2Y values obtained for the PLS model built by considering the full voltammogram (-0.8 to -1.7 V); E) Density plot of the 1000 permutated Q^2Y values obtained for the PLS model built by considering the interval -1.2/-1.4 V. The arrow indicates the Q^2Y obtained for the model.

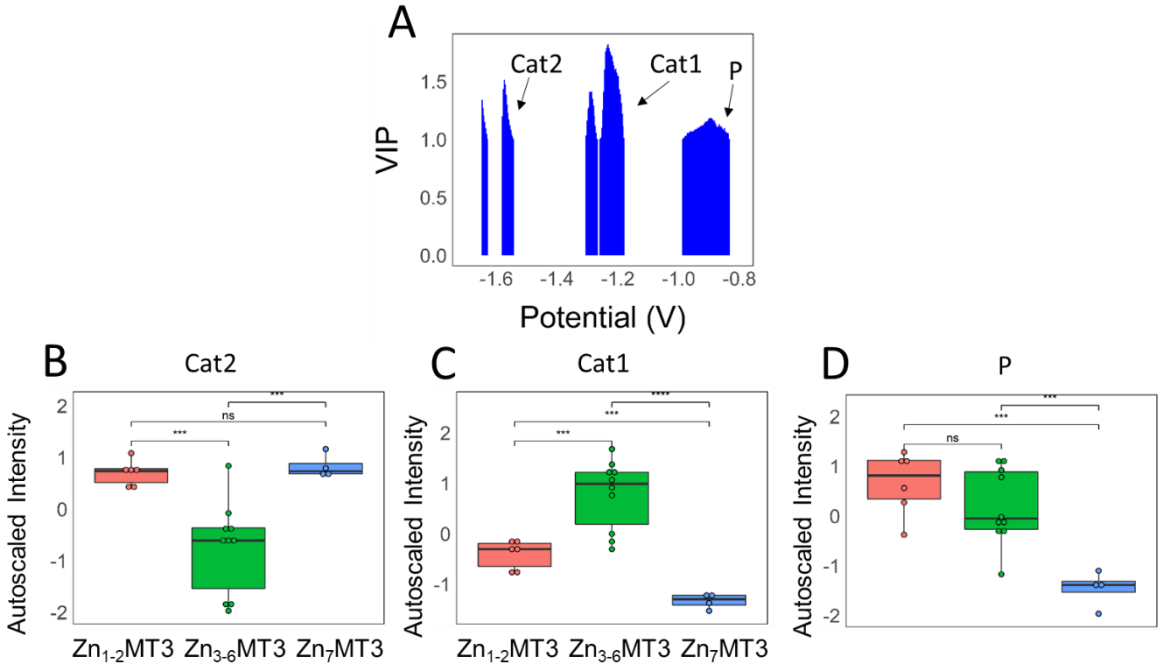

Figure 5. Variable importance in the projection (VIP) analysis of the PLS models for the autoscaled voltammograms from the $Zn_{1–7}MT3$ proteins. A) VIP plot with selected potential values holding a VIP value higher than one; B) Box-plots of the Cat2 peak highlighted by the VIP plot for the three groups: $Zn_{1–2}MT3$, $Zn_{3–6}MT3$ and Zn_7MT3; C) Box-plots of the Cat1 peak highlighted by the VIP plot for the three groups: $Zn_{1–2}MT3$, $Zn_{3–6}MT3$ and Zn_7MT3; D) Box-plots of the P peak highlighted by the VIP plot for the three groups: $Zn_{1–2}MT3$, $Zn_{3–6}MT3$ and Zn_7MT3. The *y*-axis in the box plots refers to the autoscaled intensity.

References

[1] J.H.R. Kagi, A. Schaffer, Biochemistry of metallothionein, Biochemistry, 27 (1988) 8509-8515. 10.1021/bi00423a001

[2] A. Krezel, W. Maret, The Functions of Metamorphic Metallothioneins in Zinc and Copper Metabolism, Int. J. Mol. Sci., 18 (2017) 1-20. 10.3390/ijms18061237

[3] A. Ziller, L. Fraissinet-Tachet, Metallothionein diversity and distribution in the tree of life: a multifunctional protein, Metallomics, 10 (2018) 1549-1559. 10.1039/c8mt00165k

[4] E. Freisinger, M. Vasak, Cadmium in Metallothioneins, in: A. Sigel, H. Sigel, R.K.O. Sigel (Eds.) Cadmium: From Toxicity to Essentiality, Springer, Dordrecht, 2013, pp. 339-371.

[5] C.A. Blindauer, O.I. Leszczyszyn, Metallothioneins: unparalleled diversity in structures and functions for metal ion homeostasis and more, Nat. Prod. Rep., 27 (2010) 720-741. 10.1039/b906685n

[6] E. Artells, O. Palacios, M. Capdevila, S. Atrian, Mammalian MT1 and MT2 metallothioneins differ in their metal binding abilities, Metallomics, 5 (2013) 1397-1410. 10.1039/c3mt00123g

[7] M. Vasak, G. Meloni, Mammalian Metallothionein-3: New Functional and Structural Insights, Int. J. Mol. Sci., 18 (2017) 1-15. 10.3390/ijms18061117

[8] P. Faller, D.W. Hasler, O. Zerbe, S. Klauser, D.R. Winge, M. Vasak, Evidence for a dynamic structure of human neuronal growth inhibitory factor and for major rearrangements of its metal - Thiolate clusters, Biochemistry, 38 (1999) 10158-10167. 10.1021/bi990489c

[9] S. Krizkova, M. Kepinska, G. Emri, T. Eckschlager, M. Stiborova, P. Pokorna, Z. Heger, V. Adam, An insight into the complex roles of metallothioneins in malignant diseases with emphasis on (sub)isoforms/isoforms and epigenetics phenomena, Pharmacol. Ther., 183 (2018) 90-117. 10.1016/j.pharmthera.2017.10.004

[10] A. Krezel, W. Maret, Zinc-buffering capacity of a eukaryotic cell at physiological pZn, J. Biol. Inorg. Chem., 11 (2006) 1049-1062. 10.1007/s00775-006-0150-5

[11] W. Maret, Analyzing free zinc(II) ion concentrations in cell biology with fluorescent chelating molecules, Metallomics, 7 (2015) 202-211. 10.1039/c4mt00230j

[12] M.C. Carpenter, A.S. Shah, S. DeSilva, A. Gleaton, A. Su, B. Goundie, M.L. Croteau, M.J. Stevenson, D.E. Wilcox, R.N. Austin, Thermodynamics of Pb(II) and Zn(II) binding to MT-3, a neurologically important metallothionein, Metallomics, 8 (2016) 605-617. 10.1039/c5mt00209e

[13] A. Krezel, W. Maret, Dual nanomolar and picomolar Zn(II) binding properties of metallothionein, J. Am. Chem. Soc., 129 (2007) 10911-10921.

[14] R.A. Colvin, W.R. Holmes, C.P. Fontaine, W. Maret, Cytosolic zinc buffering and muffling: Their role in intracellular zinc homeostasis, Metallomics, 2 (2010) 306-317. 10.1039/b926662c

[15] A. Krezel, Q. Hao, W. Maret, Zinc/thiolate redox biochemistry of metallothionein and the control of zinc ion fluctuations in cell signaling, Arch. Biochem. Biophys., 463 (2007) 188-200. 10.1016/j.abb.2007.02.017

[16] A. Krezel, W.G. Maret, Thionein/metallothionein control Zn(II) availability and the activity of enzymes, J. Biol. Inorg. Chem., 13 (2008) 401-409. 10.1007/s00775-007-0330-y

[17] M. Vasak, J.H.R. Kagi, H.A.O. Hill, Zinc(II), cadmium(II), and mercury(II) thiolate transitions in metallothionein, Biochemistry, 20 (1981) 2852-2856. 10.1021/bi00513a022

[18] E.M. Martin, F.D.L. Kondrat, A.J. Stewart, J.H. Scrivens, P.J. Sadler, C.A. Blindauer, Native electrospray mass spectrometry approaches to probe the interaction between zinc and an anti-angiogenic peptide from histidine-rich glycoprotein, Sci. Rep., 8 (2018) 1-13. 10.1038/s41598-018-26924-1

[19] C.V. Robinson, Mass spectrometry: From plasma proteins to mitochondrial membranes, Proc. Natl. Acad. Sci. U. S. A., 116 (2019) 2814-2820. 10.1073/pnas.1820450116
[20] R. Beveridge, S. Covill, K.J. Pacholarz, J.M.D. Kalapothakis, C.E. MacPhee, P.E. Barran, A Mass-Spectrometry-Based Framework To Define the Extent of Disorder in Proteins, Anal. Chem., 86 (2014) 10979-10991. 10.1021/ac5027435
[21] S.L. Shirran, P.E. Barran, The use of ESI-MS to probe the binding of divalent cations to calmodulin, J. Am. Soc. Mass Spectrom., 20 (2009) 1159-1171. 10.1016/j.jasms.2009.02.008
[22] N. Potier, H. Rogniaux, G. Chevreux, A. Van Dorsselaer, Ligand-metal ion binding to proteins: Investigation by ESI mass spectrometry, in: A.L. Burlingame (Ed.) Biological Mass Spectrometry, Elsevier Academic Press Inc, San Diego, 2005, pp. 361-389.
[23] L. Alvarez, H. Gonzalez-Iglesias, M. Garcia, S. Ghosh, A. Sanz-Medel, M. Coca-Prados, The stoichiometric transition from Zn6Cu1-metallothionein to Zn7-metallothionein underlies the up-regulation of metallothionein (MT) expression: Quantitative analysis of MT-metal load in eye cells, J. Biol. Chem., 287 (2012) 28456-28469. 10.1074/jbc.M112.365015
[24] A. Drozd, D. Wojewska, M.D. Peris-Diaz, P. Jakimowicz, A. Krezel, Crosstalk of the structural and zinc buffering properties of mammalian metallothionein-2, Metallomics, 10 (2018) 595-613. 10.1039/c7mt00332c
[25] P.M. Gehrig, C.H. You, R. Dallinger, C. Gruber, M. Brouwer, J.H.R. Kagi, P.E. Hunziker, Electrospray ionization mass spectrometry of zinc, cadmium, and copper metallothioneins: Evidence for metal-binding cooperativity, Protein Sci., 9 (2000) 395-402.
[26] S.H. Chen, L.X. Chen, D.H. Russell, Metal-Induced Conformational Changes of Human Metallothionein-2A: A Combined Theoretical and Experimental Study of Metal-Free and Partially Metalated Intermediates, J. Am. Chem. Soc., 136 (2014) 9499-9508. 10.1021/ja5047878
[27] R. Jara-Biedma, R. Gonzalez-Dominguez, T. Garcia-Barrera, J. Lopez-Barea, C. Pueyo, J.L. Gomez-Ariza, Evolution of metallotionein isoforms complexes in hepatic cells of Mus musculus along cadmium exposure, Biometals, 26 (2013) 639-650. 10.1007/s10534-013-9636-0
[28] S. Kameo, K. Nakai, A. Naganuma, H. Koyama, H. Satoh, Simple analysis method for metallothionein-1, -2 and -3 in the brain by one-step size-exclusion column HPLC on-line coupling with inductively coupled plasma mass spectrometry, J. Anal. Bioanal. Tech., 5 (2014) 1-6.
[29] L. Tio, L. Villarreal, S. Atrian, M. Capdevila, Functional differentiation in the mammalian metallothionein gene family - Metal binding features of mouse MT4 and comparison with its paralog MT1, J. Biol. Chem., 279 (2004) 24403-24413. 10.1074/jbc.M401346200
[30] G.T.H. Nguyen, T.N. Tran, M.N. Podgorski, S.G. Bell, C.T. Supuran, W.A. Donald, Nanoscale Ion Emitters in Native Mass Spectrometry for Measuring Ligand-Protein Binding Affinities, ACS Central Sci., 5 (2019) 308-318. 10.1021/acscentsci.8b00787
[31] Y. Kostyukevich, A. Kononikhin, I. Popov, M. Indeykina, S.A. Kozin, A.A. Makarov, E. Nikolaev, Supermetallization of peptides and proteins during electrospray ionization, J. Mass Spectrom., 50 (2015) 1079-1087. 10.1002/jms.3622
[32] H. Mattapalli, W.B. Monteith, C.S. Burns, A.S. Danell, Zinc Deposition During ESI-MS Analysis of Peptide-Zinc Complexes, J. Am. Soc. Mass Spectrom., 20 (2009) 2199-2205. 10.1016/j.jasms.2009.08.007
[33] I. Sestáková, T. Navrátil, Voltammetric methods in metallothionein research, Bioinorg Chem Appl, 3 (2005) 43-53. 10.1155/BCA.2005.43
[34] M.J. López, C. Ariño, S. Díaz-Cruz, J.M. Díaz-Cruz, R. Tauler, M. Esteban, Voltammetry Assisted by Multivariate Analysis as a Tool for Speciation of Metallothioneins: Competitive Complexation of α- and β-Metallothionein Domains with Cadmium and Zinc, Environmental Science & Technology, 37 (2003) 5609-5616. 10.1021/es030048n

[35] A. Cardova, P. Adam, S. Mariani, L. Richtera, Z. Heger, J. Labuda, M. Minunni, V. Adam, Electrochemical and optical study of metallothionein interactions with prion proteins, J. Pharm. Biomed. Anal., 140 (2017) 355-361. 10.1016/j.jpba.2017.03.044
[36] W.H. Fan, X.R. Wang, X.M. Li, F. Xue, Determination of metallothionein in Daphnia magna by modified square wave cathodic stripping voltammetry, Electrochem. Commun., 52 (2015) 17-20. 10.1016/j.elecom.2015.01.008
[37] D. Krivska, I. Sestakova, J. Szakova, Z. Cadkova, Z. Kotikova, I. Langrova, Sample handling and pretreatment as critical points in determining the quality of analytical data during metallothionein determination in wild animals, Ecol. Indic., 98 (2019) 214-217. 10.1016/j.ecolind.2018.11.002
[38] M. Esteban, C. Harlyk, A.R. Rodríguez, Cadmium binding properties of the C-terminal hexapeptide from mouse metallothionein: study by linear sweep voltammetry and multivariate curve resolution analysis, J. Electroanal. Chem., 468 (1999) 202-212. https://doi.org/10.1016/S0022-0728(99)00176-X
[39] J. Petrlova, D. Potesil, R. Mikelova, O. Blastik, V. Adam, L. Trnkova, F. Jelen, R. Prusa, J. Kukacka, R. Kizek, Attomole voltammetric determination of metallothionein, Electrochim. Acta, 51 (2006) 5112-5119. 10.1016/j.electacta.2006.03.078
[40] B. Raspor, M. Paic, M. Erk, Analysis of metallothioneins by the modified Brdicka procedure, Talanta, 55 (2001) 109-115. 10.1016/s0039-9140(01)00399-x
[41] S. Krizkova, P. Blahova, J. Nakielna, I. Fabrik, V. Adam, T. Eckschlager, M. Beklova, Z. Svobodova, V. Horak, R. Kizek, Comparison of Metallothionein Detection by Using Brdicka Reaction and Enzyme-Linked Immunosorbent Assay Employing Chicken Yolk Antibodies, Electroanalysis, 21 (2009) 2575-2583. 10.1002/elan.200900243
[42] V. Adam, S. Krizkova, O. Zitka, L. Trnkova, J. Petrlova, M. Beklova, R. Kizek, Determination of apo-metallothionein using adsorptive transfer stripping technique in connection with differential pulse voltammetry, Electroanalysis, 19 (2007) 339-347. 10.1002/elan.200603738
[43] I. Fabrik, Z. Ruferova, K. Hilscherova, V. Adam, L. Trnkova, R. Kizek, A determination of metallothionein in larvae of freshwater midges (Chironomus riparius) using Brdicka reaction, Sensors, 8 (2008) 4081-4094. 10.3390/s8074081
[44] D. Huska, I. Fabrik, J. Baloun, V. Adam, M. Masarik, J. Hubalek, A. Vasku, L. Trnkova, A. Horna, L. Zeman, R. Kizek, Study of Interactions between Metallothionein and Cisplatin by using Differential Pulse Voltammetry Brdicka's reaction and Quartz Crystal Microbalance, Sensors, 9 (2009) 1355-1369. 10.3390/s90301355
[45] M. Kepinska, S. Krizkova, E. Guszpit, M.A.M. Rodrigo, H. Milnerowicz, The application of capillary electrophoresis, mass spectrometry and Brdicka reaction in human and rabbit metallothioneins analysis, Adv. Clin. Exp. Med., 27 (2018) 1601-1608. 10.17219/acem/98916
[46] J. Kovarova, R. Kizek, V. Adam, D. Harustiakova, O. Celechovska, Z. Svobodova, Effect of Cadmium Chloride on Metallothionein Levels in Carp, Sensors, 9 (2009) 4789-4803. 10.3390/s90604789
[47] M. Ryvolova, D. Hynek, H. Skutkova, V. Adam, I. Provaznik, R. Kizek, Structural changes in metallothionein isoforms revealed by capillary electrophoresis and Brdicka reaction, Electrophoresis, 33 (2012) 270-279. 10.1002/elps.201100312
[48] V. Adam, D. Chudobova, K. Tmejova, K. Cihalova, S. Krizkova, R. Guran, M. Kominkova, M. Zurek, M. Kremplova, A.M.J. Jimenez, M. Konecna, D. Hynek, V. Pekarik, R. Kizek, An Effect of Cadmium and Lead Ions on Escherichia coli with the Cloned Gene for Metallothionein (MT-3) Revealed by Electrochemistry, Electrochim. Acta, 140 (2014) 11-19. 10.1016/j.electacta.2014.06.091

[49] S.H. Hong, M. Toyama, W. Maret, Y. Murooka, High yield expression and single step purification of human thionein/metallothionen, Protein Expr. Purif., 21 (2001) 243-250. 10.1006/prep.2000.1372
[50] A. Krezel, R. Latajka, G.D. Bujacz, W. Bal, Coordination properties of tris(2-carboxyethyl)phosphine, a newly introduced thiol reductant, and its oxide, Inorg. Chem., 42 (2003) 1994-2003. 10.1021/ic025969y
[51] P. Eyer, F. Worek, D. Kiderlen, G. Sinko, A. Stuglin, V. Simeon-Rudolf, E. Reiner, Molar absorption coefficients for the reduced Ellman reagent: reassessment, Anal. Biochem., 312 (2003) 224-227. 10.1016/s0003-2697(02)00506-7
[52] A. Kocyla, A. Pomorski, A. Krezel, Molar absorption coefficients and stability constants of metal complexes of 4-(2-pyridylazo)resorcinol (PAR): Revisiting common chelating probe for the study of metalloproteins, J. Inorg. Biochem., 152 (2015) 82-92. 10.1016/j.jinorgbio.2015.08.024
[53] R.A. van den Berg, H.C.J. Hoefsloot, J.A. Westerhuis, A.K. Smilde, M.J. van der Werf, Centering, scaling, and transformations: improving the biological information content of metabolomics data, BMC Genomics, 7 (2006) 1-15. 10.1186/1471-2164-7-142
[54] T. Fearn, C. Riccioli, A. Garrido-Varo, J.E. Guerrero-Ginel, On the geometry of SNV and MSC, Chemometrics Intell. Lab. Syst., 96 (2009) 22-26. 10.1016/j.chemolab.2008.11.006
[55] A. Savitzky, M.J.E. Golay, Smoothing and differentiation of data by simplified least squares procedures, Anal. Chem., 36 (1964) 1627-1639. 10.1021/ac60214a047
[56] M.D. Peris-Diaz, B. Lydzba-Kopczynska, E. Sentandreu, Raman spectroscopy coupled to chemometrics to discriminate provenance and geological age of amber, J. Raman Spectrosc., 49 (2018) 842-851. 10.1002/jrs.5357
[57] R. Bro, A.K. Smilde, Principal component analysis, Anal. Methods, 6 (2014) 2812-2831. 10.1039/c3ay41907j
[58] S. Wold, M. Sjostrom, L. Eriksson, PLS-regression: a basic tool of chemometrics, Chemometrics Intell. Lab. Syst., 58 (2001) 109-130. 10.1016/s0169-7439(01)00155-1
[59] M. Andersson, A comparison of nine PLS1 algorithms, J. Chemometr., 23 (2009) 518-529. 10.1002/cem.1248
[60] M. Barker, W. Rayens, Partial least squares for discrimination, J. Chemometr., 17 (2003) 166-173. 10.1002/cem.785
[61] R.G. Brereton, G.R. Lloyd, Partial least squares discriminant analysis: taking the magic away, J. Chemometr., 28 (2014) 213-225. 10.1002/cem.2609
[62] E. Szymanska, E. Saccenti, A.K. Smilde, J.A. Westerhuis, Double-check: validation of diagnostic statistics for PLS-DA models in metabolomics studies, Metabolomics, 8 (2012) S3-S16. 10.1007/s11306-011-0330-3
[63] C.M. Andersen, R. Bro, Variable selection in regression-a tutorial, J. Chemometr., 24 (2010) 728-737. 10.1002/cem.1360
[64] B.H. Mevik, R. Wehrens, The pls package: Principal component and partial least squares regression in R, J. Stat. Softw., 18 (2007) 1-23.
[65] H. Wickham, ggplot2: Elegant Graphics for Data Analysis, Springer Publishing Company2009.
[66] P. Sobrova, L. Vyslouzilova, O. Stepankova, M. Ryvolova, J. Anyz, L. Trnkova, V. Adam, J. Hubalek, R. Kizek, Tissue Specific Electrochemical Fingerprinting, PLoS One, 7 (2012) 1-12. 10.1371/journal.pone.0049654
[67] A. Arseniev, P. Schultze, E. Worgotter, W. Braun, G. Wagner, M. Vasak, J.H.R. Kagi, K. Wuthrich, 3-dimensional structure of rabbit liver [Cd7]metallothionein-2a in aqueous solution determined by nuclear magnetic resonance, J. Mol. Biol., 201 (1988) 637-657. 10.1016/0022-2836(88)90644-4

[68] M. Good, R. Hollenstein, M. Vasak, Metal selectivity of clusters in rabbit liver metallothionein, Eur. J. Biochem., 197 (1991) 655-659. 10.1111/j.1432-1033.1991.tb15955.x
[69] L. Norgaard, A. Saudland, J. Wagner, J.P. Nielsen, L. Munck, S.B. Engelsen, Interval partial least-squares regression (iPLS): A comparative chemometric study with an example from near-infrared spectroscopy, Appl. Spectrosc., 54 (2000) 413-419. 10.1366/0003702001949500
[70] M. Jakubowska, Signal Processing in Electrochemistry, Electroanalysis, 23 (2011) 553-572. 10.1002/elan.201000465